ELSEVIER

Quaternary Science Reviews 26 (2007) 82–97

QSR

Solar activity during the last 1000 yr inferred from radionuclide records

Raimund Muscheler[a,*], Fortunat Joos[b], Jürg Beer[c], Simon A. Müller[b], Maura Vonmoos[c], Ian Snowball[d]

[a]NASA/Goddard Space Flight Center, Climate & Radiation Branch, Mail Code 613.2, Building 33, Room C327, Greenbelt, MD 20771, USA
[b]Climate and Environmental Physics, Physics Institute, University of Bern, Sidlerstr. 5, CH-3012 Bern, Switzerland
[c]Swiss Federal Institute of Aquatic Science and Technology (EAWAG), Ueberlandstrasse 133, CH-8600 Dübendorf, Switzerland
[d]GeoBiosphere Science Centre, Quaternary Sciences, Lund University, Sölvegatan 12, 22362 Lund, Sweden

Received 12 March 2006; accepted 21 July 2006

Abstract

Identification of the causes of past climate change requires detailed knowledge of one of the most important natural factors—solar forcing. Prior to the period of direct solar observations, radionuclide abundances in natural archives provide the best-known proxies for changes in solar activity. Here we present two independent reconstructions of changes in solar activity during the last 1000 yr, which are inferred from ^{10}Be and ^{14}C records. We analyse the tree-ring ^{14}C data (SHCal, IntCal04 from 1000 to 1510 AD and annual data from 1511 to 1950 AD) and four ^{10}Be records from Greenland ice cores (Camp Century, GRIP, Milcent and Dye3) together with two ^{10}Be records from Antarctic ice cores (Dome Concordia and South Pole). In general, the ^{10}Be and ^{14}C records exhibit good agreement that allows us to obtain reliable estimates of past solar magnetic modulation of the radionuclide production rates. Differences between ^{10}Be records from Antarctica and Greenland indicate that climatic changes have influenced the deposition of ^{10}Be during some periods of the last 1000 yr. The radionuclide-based reconstructions of past changes in solar activity do not always agree with the sunspot record, which indicates that the coupling between those proxies is not as close as has been sometimes assumed. The tree-ring ^{14}C record and ^{10}Be from Antarctica indicate that recent solar activity is high but not exceptional with respect to the last 1000 yr.

1. Introduction

To study the solar influence on climate it is crucial to know how the activity of the Sun changed in the past. Cosmogenic radionuclide records provide the most reliable known proxies for changes in solar activity that occurred before the period of direct solar observations. Time dependent variations in such proxies have been used to infer a solar influence on climate by comparison with climate reconstructions (Bond et al., 2001; Denton and Karlén, 1973). However, changes in cosmogenic radionuclide records are not exclusively the result of the variable Sun. The strength and direction of the geomagnetic field also influences the production rates of the cosmogenic radionuclides and changes in climate can potentially influence the transport of the cosmogenic radionuclides from the atmosphere into the natural archives where they are stored. The disagreement between two reconstructions of solar activity during the last approximately 1000 yr (Bard et al., 2000; Usoskin et al., 2003) demonstrates the problems associated with identifying and separating these climatic and geomagnetic influences. While Bard et al. (2000) conclude that solar activity at around 1200 AD was similar to, or even higher than at present, Usoskin et al. (2003) suggest that solar activity reached a distinct maximum during the last 60 yr, which was significantly higher than during the preceding 1000 yr. Solanki et al. (2004) go even further and suggest that the level of solar activity during the past 70 yr was exceptional compared to the preceding 8000 yr.

In the following we will combine the available information from cosmogenic radionuclide, neutron and

*Corresponding author. Tel.: +1 301 614 6213; fax: +1 301 614 6307.
E-mail addresses: raimund@climate.gsfc.nasa.gov (R. Muscheler), joos@climate.unibe.ch (F. Joos), beer@eawag.ch (J. Beer), smueller@climate.unibe.ch (S.A. Müller), maura.vonmoos@eawag.ch (M. Vonmoos), Ian.Snowball@geol.lu.se (I. Snowball).

0277-3791/$ - see front matter © 2006 Elsevier Ltd. All rights reserved.
doi:10.1016/j.quascirev.2006.07.012

geomagnetic field records to identify and illustrate the uncertainties in the different records and to obtain a reliable estimate of past changes in solar activity during the last 1000 yr. The first part describes the theoretical basis of the radionuclide-based reconstruction of solar activity. It is followed by a discussion of the geomagnetic influence on the cosmogenic radionuclide production. We infer the history of changes in solar modulation from the tree-ring ^{14}C record and these changes are subsequently compared to an independent ^{10}Be-based reconstruction of solar modulation. The errors are calculated from the uncertainties and differences between and within the individual records used for these calculations. The last part is dedicated to a comparison with the sunspot and irradiance records.

2. The production, transport and deposition mechanisms of ^{10}Be and ^{14}C

2.1. The production of ^{10}Be and ^{14}C

Cosmogenic radionuclides are produced in the Earth's atmosphere in the cascades of nuclear reactions induced by the high-energy galactic cosmic rays (GCRs, Lal and Peters, 1967; Masarik and Beer, 1999). Therefore, the productions of ^{10}Be and ^{14}C in the atmosphere have the same cause but the processes leading to them are slightly different. ^{10}Be is mainly produced by spallation reactions when high-energy particles hit oxygen and nitrogen in the atmosphere (Lal and Peters, 1967). By reacting with nitrogen in the atmosphere slower (thermal) neutrons originating from secondary reactions are mainly responsible for the ^{14}C production (Lal and Peters, 1967).

The Sun influences the radionuclide production rate indirectly by modulating the GCR flux reaching the Earth's atmosphere. In general, lower magnetic field intensity carried by the solar wind (and lower geomagnetic dipole field intensity) leads to a higher CGR flux to the Earth's atmosphere and higher production rates of cosmogenic radionuclides. While the GCR transport in the heliosphere is complicated the force-field approximation is a simplification that parameterises the solar modulation with a single parameter, the so-called modulation function Φ (Gleeson and Axford, 1968). This method gives a good approximation for the cosmic ray spectrum in the inner heliosphere, which is the cosmic ray spectrum impinging on the Earth's atmosphere (Caballero-Lopez and Moraal, 2004). Masarik and Beer (1999) calculated the ^{10}Be and ^{14}C production rates in the Earth's atmosphere using the force-field approximation and the local interstellar cosmic ray spectrum (LIS) suggested by Cini Castagnoli and Lal (1980). Fig. 1 shows how the globally averaged ^{14}C production rate depends on the geomagnetic dipole field intensity and the solar modulation function Φ (Masarik and Beer, 1999). High values of Φ signify strong magnetic fields enclosed in the solar wind, the strong deflection of galactic cosmic rays and relatively low production rates of

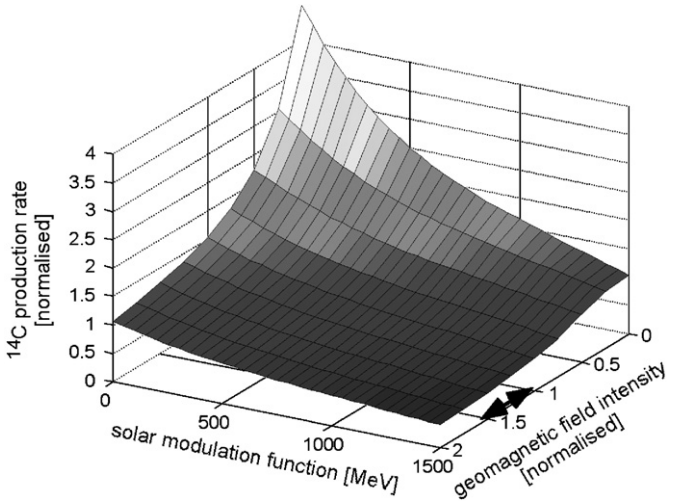

Fig. 1. Normalised ^{14}C production rate depending on the solar modulation function and the geomagnetic dipole field intensity (Masarik and Beer, 1999). The geomagnetic field intensity is normalised with respect to today's value. The arrow placed along the geomagnetic field axis indicates the range of variability derived from geomagnetic field reconstructions and observations for the last 1000 yr (see Fig. 2).

cosmogenic radionuclides in the Earth's atmosphere. Conversely, low values of Φ correspond to periods of a "quiet Sun" and relatively high rates of cosmogenic radionuclide production. A solar modulation function of 0 is the lowest limit since it means absent solar shielding of galactic cosmic rays. The calculations of Masarik and Beer (1999) comprise Φ values from 0 to 1000 MeV. However, during the last 50 yr the solar modulation went up to $\Phi = 1200$ MeV (Masarik and Beer, 1999). Since the plane in Fig. 1 becomes very flat for large Φ values it can be extrapolated to higher values. Here, we chose a linear extrapolation which could slightly overestimate the production rate changes for $\Phi > 1000$ MeV. In general, the ^{10}Be production rate reacts in a very similar way as ^{14}C to changes in solar and geomagnetic shielding (Masarik and Beer, 1999). However, due to the different production processes the ^{10}Be production rate responds less sensitively to changes in the solar magnetic field than ^{14}C. For example, at the present level of geomagnetic field intensity a solar activity change that induces a 10% increase in the ^{10}Be production rate causes the ^{14}C production rate to increase by 13%. Since Masarik and Beer (1999) did not include the differences in the solar modulation of protons and heavier particles in the GCRs they underestimated slightly the amplitude of the solar-induced variations (McCracken, 2004). In addition, new measurements for the LIS suggest revisions to the LIS adopted by Masarik and Beer (Webber and Higbie, 2003). Webber and Higbie (2003) included these improvements in their calculations of the ^{10}Be production rate in polar regions. They suggest an approximately 10% higher increase in the ^{10}Be production rate for absent solar modulation. In general, the differences are much smaller. Since Masarik and Beer (1999) also calculated the ^{10}Be and ^{14}C production rates for different

latitudes we will use their results throughout the following calculations but we have to keep in mind that they could slightly underestimate the ^{10}Be and ^{14}C production changes for low solar modulation.

2.2. Transport and deposition of ^{10}Be and ^{14}C

More important for geophysical applications, however, is the completely different geo-chemical behaviour of ^{10}Be compared to ^{14}C. After production ^{10}Be attaches to aerosols and is removed from the atmosphere after an average residence time of 1–2 yr (McHargue and Damon, 1991; Raisbeck et al., 1981). At least part of the ^{10}Be deposition is expected to reflect the global ^{10}Be production since more than 50% of ^{10}Be is produced in the stratosphere. Due to the much shorter atmospheric residence time in the troposphere, the tropospheric ^{10}Be component could be influenced by local atmospheric circulation patterns. For ^{10}Be data from polar ice cores this could imply that the solar-induced variations in ^{10}Be are amplified due to the almost absent geomagnetic shielding at the geographic poles (the movement of the geomagnetic poles is insignificant at the timescales considered here). New results from general circulation model calculations suggest that this could indeed be the case (Field et al., 2006). Changes in deposition due to variable precipitation could also add a climatic component to the measured ^{10}Be concentration (Wagner et al., 2001). Since the atmospheric transport and deposition of ^{10}Be is not yet well understood we have to rely on rather simple assumptions to reconstruct the ^{10}Be production rate based on measured ^{10}Be concentrations in ice cores.

By contrast, radiocarbon in the atmosphere is much less prone to local effects. After production ^{14}C oxidizes to $^{14}CO_2$ and stays in a gaseous phase. The relatively long atmospheric residence time of approximately 5 yr ensures that $^{14}CO_2$ is well mixed within each hemisphere. However, radiocarbon is also redistributed among the carbon reservoirs in the atmosphere, on land and in the ocean. Changes in atmospheric radiocarbon concentration can be attributed to variations in the ^{14}C production rate and changes in the global carbon cycle (Siegenthaler et al., 1980). For example, it is well known that the atmospheric radiocarbon record over the industrial period is influenced by the release of radiocarbon-free fossil fuel CO_2 (Suess, 1953). The combustion of fossil carbon has significantly reduced the $^{14}C/^{12}C$ ratios in the atmosphere, biosphere and the ocean, and this reduction is called the Suess effect. Changes in the exchange rates between and within the ^{14}C reservoirs can also alter the $^{14}C/^{12}C$ ratio in the atmosphere. Variations in oceanic ventilation are potentially the most important cause of natural variations in the atmospheric ^{14}C concentration related to the carbon cycle (Siegenthaler et al., 1980). The annual ^{14}C production is relatively small compared to the ^{14}C content in the atmosphere, biosphere and ocean. Due to these large ^{14}C reservoirs and the permanent CO_2 exchange between them short-term variations in the ^{14}C production appear strongly dampened in atmospheric ^{14}C concentration (Siegenthaler et al., 1980). As a consequence, to reconstruct past changes in solar activity with radiocarbon one has to account for the redistribution of ^{14}C within the Earth system by using a carbon cycle model.

To summarise, ^{10}Be and ^{14}C both have advantages and disadvantages as proxies for solar activity. By comparing the different records it is possible to identify periods when the records are influenced by changes in climate, which are the largest uncertainty affecting the interpretation of these records. In the following we will discuss and compare the different data sets that are necessary to reconstruct solar activity changes based on cosmogenic radionuclide data.

3. The geomagnetic influence

Fig. 1 shows that the cosmogenic radionuclide production rate depends in a non-linear way upon geomagnetic and solar magnetic shielding. While there is no question that internally driven changes in geomagnetic dipole field intensity significantly influence cosmogenic radionuclide production rates on time scales longer than 2000–3000 yr (Wagner et al., 2000), it has also been proposed that geomagnetic field changes on centennial time scales could contribute significantly to the variability of the radionuclide production rate (Snowball and Sandgren, 2002; St-Onge et al., 2003). However, the observed and reconstructed range of short-term geomagnetic variability during the last 1000 yr is limited and, therefore, geomagnetic field intensity changes can only explain a relatively small fraction of the changes in the cosmogenic radionuclide production rate. Nevertheless, the limited temporal resolution of paleomagnetic data and differences between alternative geomagnetic field reconstructions remain major sources of uncertainty for estimates of past changes in solar activity.

Fig. 2 shows different reconstructions of past changes in geomagnetic dipole field intensity (Valet, 2003 and references therein). Almost all records displayed in Fig. 2 show a long-term decrease in geomagnetic dipole field intensity during the last 1000 yr. The short-term changes in geomagnetic field intensity that are present in the different records could have impacts on the production rates of cosmogenic radionuclides. However, the differences between the geomagnetic field records suggest that (i) local effects due to higher moments of the geomagnetic field significantly influence the individual records, (ii) there is analytical "noise" in the reconstructions or (iii) the records suffer from random dating errors. Efforts to include all available data to construct a model of the global geomagnetic field behaviour have to a certain extent overcome some of the problems associated with local records (Korte and Constable, 2005) but the southern hemisphere is under-represented compared to the northern hemisphere. Since the cosmic ray modulation is most important far away from the Earth's surface, where the

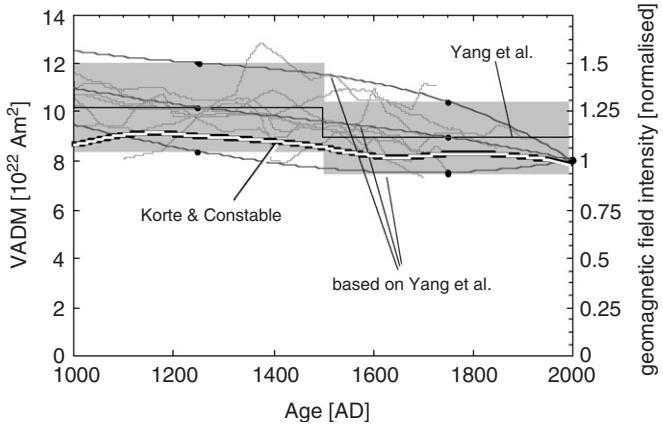

Fig. 2. Different reconstructions of the changes in geomagnetic field intensity during the last 1000 yr. The thin grey curves show archaeomagnetic data from Bulgaria, the Caucasus, Ukraine, Japan and composite records (Valet, 2003 and references therein). The thick black curve band shows an estimate of global changes in geomagnetic field intensity based on archaeomagnetic data (Yang et al., 2000). The thick grey curves show the geomagnetic field record including the error range based on Yang et al. (2000) that was used for the reconstruction of the solar magnetic modulation. The white line shows the results of a spherical harmonic model calculation that includes archaeomagnetic and sediment data to reconstruct the global geomagnetic dipole field (Korte and Constable, 2005).

higher moments of the geomagnetic field do not significantly contribute to the shielding, the cosmogenic radionuclide production rate in the atmosphere is predominantly influenced by the geomagnetic dipole moment.

The black line in Fig. 2 shows the compilation of archaeomagnetic data (Yang et al., 2000). The underlying data are numerous and widely distributed over the northern hemisphere so their average is considered to be a relative precise estimate of the dipole field intensity. However, due to the necessary averaging process potential short-term changes are removed and only 500 yr averages of the field intensity were obtained by this method (Yang et al., 2000). Since the step function provided by Yang et al. (2000) is not a realistic representation of the real time evolution of the geomagnetic field we used the mid points of the averaged intensity including the present field value of 8×10^{22} Am^2 to fit a third-order polynomial to the intensity values. The mean reconstructed geomagnetic field decreases by approximately 5% during the last century, which is in accordance with instrumental measurements (Valet, 2003). Potential short-term changes in the global geomagnetic dipole field that are removed by this reconstruction of the geomagnetic field intensity could influence the cosmogenic radionuclide production rate. We account for this uncertainty by including the relatively large error band (see Fig. 2) in the following calculations. The white line in Fig. 2 shows the results of a new method to combine the available geomagnetic field data and to construct the global geomagnetic dipole field and its changes (Korte and Constable, 2005). It suggests smaller changes in geomagnetic dipole field intensity during the last 1000 yr than those indicated by Yang et al. (2000).

4. The interpretation of Δ^{14}C records in terms of production and solar modulation

4.1. The Δ^{14}C data

The following calculations of the ^{14}C production rate are based on the tree-ring Δ^{14}C records shown in Fig. 3a and three different carbon cycle models. Δ^{14}C is defined as the per mil deviation from the National Institute of Standards and Technology ^{14}C/^{12}C standard after correction for decay and fractionation (Stuiver and Polach, 1977). Two records in Fig. 3a are derived from tree-ring measurements from the northern hemisphere, which reflect past changes in the atmospheric ^{14}C concentration. The lower-resolution part before 1500 AD is from the IntCal04 calibration curve (Reimer et al., 2004). From 1511 to 1950 AD there are annual Δ^{14}C data published by Stuiver et al. (Stuiver and Braziunas, 1993; Stuiver et al., 1998). A third curve shows the Δ^{14}C development in the southern hemisphere (SHCal04) (McCormac et al., 2004). The ^{14}C record from the mid-1950s to today cannot be used for this analysis since nuclear bomb tests released large amounts of artificial ^{14}C into the atmosphere (counteracting the Suess effect) and the budget of this bomb-produced radiocarbon is uncertain (Joos, 1994).

4.2. Modelling the ^{14}C production rate

With carbon cycle models it is possible to reconstruct the ^{14}C production rate from tropospheric Δ^{14}C data (Stuiver

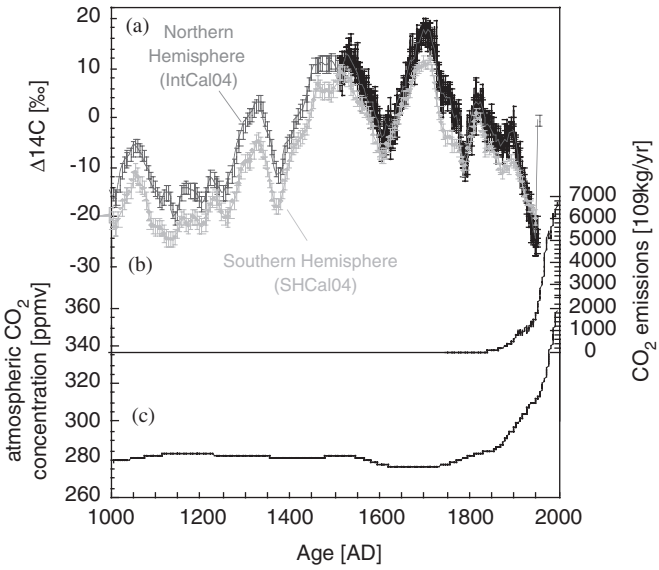

Fig. 3. Evolution of atmospheric ^{14}C (a), fossil CO_2 emissions (b) (Marland et al., 2003) and atmospheric CO_2 concentration (c) (Etheridge et al., 1996). Panel a shows two records from the northern hemisphere (black and dark grey (Reimer et al., 2004; Stuiver and Braziunas, 1993; Stuiver et al., 1998) and a record from the southern hemisphere (McCormac et al., 2004). The fossil CO_2 emissions represent an input of ^{14}C-free ("dead") carbon into the atmosphere that partly causes the Δ^{14}C drop in the first part of the 20th century (Suess effect).

and Quay, 1980). The Suess effect can be taken into account by including the anthropogenic CO_2 emissions shown in Fig. 3b (Marland et al., 2003). Potential unidentified changes in the carbon cycle lead to uncertainties in the reconstructed ^{14}C production rate. However, such changes are expected to be small during relatively stable climatic periods (Muscheler et al., 2004a; Siegenthaler et al., 1980). The results at the beginning of the model run can be affected by the choice of the starting conditions. For example, starting with a too high ^{14}C inventory in the model reservoirs results in a too low ^{14}C production rate during the first millennia of the calculation (Muscheler et al., 2005a). To avoid such artefacts we set our model to start several millennia before the present. The annual tree-ring $\Delta^{14}C$ data shows short-term changes that cannot be completely explained by changes in ^{14}C production rate since the scatter in the data would lead to unrealistic changes in the ^{14}C production rate. The observed inter-annual variability in tropospheric ^{14}C is more likely produced by inter-annual variability in the exchange between the various carbon reservoirs (ocean, land, stratosphere and troposphere) or simply by the measurement uncertainties that are in most cases larger than the annual changes (Stuiver et al., 1998). In addition, the typical inter-hemispheric exchange time and the stratosphere–troposphere exchange time is several years for ^{14}C (Siegenthaler et al., 1980). Therefore, a global carbon cycle model, which includes only one box for the atmosphere, can only be reasonably applied to data with a time resolution of a few years or longer. For the calculations that use the annual data we low-pass filtered our $\Delta^{14}C$ records with a cut-off frequency of $1/8\,yr^{-1}$ before calculating the ^{14}C production rate. This filter insures that we include one of the most important features of the variable cosmogenic radionuclide production rate, the 11-yr cycle.

To assess the reliability of our results we used three different carbon cycle models: The outcrop-diffusion (OD) carbon cycle model, the HILDA model and the Bern3D carbon cycle model. The calculations with the OD carbon cycle model proposed by Siegenthaler (1983) are described by Muscheler et al. (2005a). The model calibration with no direct exchange between the atmosphere and the deep sea is used ($a_c = 0.0$; $K = 4005\,m^2\,yr^{-1}$; $F_{as} = 18.0\,mol\,m^{-2}\,yr^{-1}$; see Siegenthaler, 1983). The terrestrial biosphere was treated as a single box. The ^{14}C production rate was reconstructed under the assumption that the carbon cycle was stable until 1850 AD. After 1850 AD the anthropogenic release of CO_2 was included in the calculation. The difference between the $\Delta^{14}C$ records from the northern and southern hemispheres was included in the calculations by averaging the $\Delta^{14}C$ record from the two hemispheres. We retained the annual resolution from 1511 AD onwards by subtracting a correction function (annually interpolated) inferred from the IntCal04 and SHCal04 difference from the annual record. The past ^{14}C production rate was reconstructed by continually adjusting the ^{14}C production rate to obtain agreement between model output and observed atmospheric ^{14}C changes. For example, if the modelled $\Delta^{14}C$ output was lower than the measured value the method automatically increased the ^{14}C production rate according to the difference. This method produces very reliable results since the measured $\Delta^{14}C$ can be very well reproduced (Muscheler, 2000). A Monte-Carlo approach was used to account for the propagation of the errors in the radiocarbon record. According to the errors specified in the original $\Delta^{14}C$ record we randomly added such deviations to the mean $\Delta^{14}C$ values. After that we applied the low-pass filter ($1/8\,yr^{-1}$) and calculated the ^{14}C production rate. This was done 100 times and from the resulting curves we calculated the average ^{14}C production rate and the corresponding errors.

Calculations were also performed with the high latitude exchange/interior diffusion-advection (HILDA) model (Siegenthaler and Joos, 1992; Joos et al., 1996) coupled to a four-box terrestrial biosphere component using their impulse response function (IRF) representation (Joos et al., 1996). Between 1006 AD and 1950 AD atmospheric CO_2 was prescribed in the model using a smoothing spline function fitted to the Law Dome CO_2 ice core record (Enting, 1987; Etheridge et al., 1996). CO_2 was kept constant prior to 1006 AD as the Holocene CO_2 variations of 20 ppm are of minor relevance to the calculations here. The carbon balance was closed by inferring a land use source (sink) from the difference in the prescribed change in atmospheric carbon inventory and the modelled change in ocean carbon inventory and the modelled carbon uptake by the land biota minus the prescribed emissions (Marland et al., 2003) from fossil fuel burning and cement production (Bruno and Joos, 1997). Atmospheric $\Delta^{14}C$ was prescribed in the model using the IntCal04 data set averaged with the data from the southern hemisphere (SHCal) (Reimer et al., 2004; McCormac et al., 2004). The radiocarbon production rate was inferred at each model time step as the sum of the net radiocarbon fluxes into the ocean and the land biosphere, taking into account gross and net exchange fluxes of carbon (see e.g. Joos and Bruno, 1998), and the decay of ^{14}C in the atmosphere. The IRF approach is a perturbation approach and simulations were started 25,000 yr ago to take into account the history of the atmospheric radiocarbon production.

The air–sea gas exchange coefficients for carbon and other gases are uncertain and different estimates vary by a factor of two. The sensitivity of the inferred ^{14}C production rate to this parameter was investigated by varying the gas exchange rate in the HILDA model (1/9.06 yr with respect to the atmospheric carbon inventory) by $\pm 30\%$. Differences in the long-term (500 yr average) production rate are 2%. Differences in the 20-yr averaged production rates are up to about 15% for the last 1000 yr, when production varied between 50% and 140% relative to the average of the past 500 yr. Thus, results are relatively insensitive to the exact choice of the gas exchange parameter. The exchange rate between the ocean surface and deeper layers is not well

known either. However, the results for the inferred ^{14}C production rate do not depend on the applied carbon cycle model which indicates that these uncertainties do not strongly influence our results.

We also applied the Bern3D ocean model to further investigate the influence of hemispheric differences and prescribed the northern hemisphere (IntCal04) record at northern latitudes and the southern data (SHCal04) south of the equator. The Bern3D ocean model (Müller et al., in press) is a cost-efficient geostrophic-frictional balance ocean model. It was complemented with formulations describing the cycling of carbon and its isotopes similar to those described by Marchal et al. (1998) and used in the Ocean Carbon Cycle Model Intercomparison Project, phase II (Orr, 1999). Thus, in contrast to the OD and the HILDA model, which are based on perturbation formulations for anthropogenic carbon only, the Bern3D model includes the natural carbon cycle and a realistic total carbon inventory. The model was coupled to a well-mixed atmosphere and the four-box biosphere of Siegenthaler and Oeschger (1987). The land biosphere was forced by the northern hemisphere $\Delta^{14}C$ data only, as most of the terrestrial biosphere is located in the north. A spline fit through an updated ice core CO_2 record over the last 5500 yr (Siegenthaler et al., 2005; Etheridge et al., 1996) and fossil emissions were prescribed and the carbon budget for the atmosphere was closed by inferring land use emissions. The radiocarbon production rate was calculated from the ^{14}C content changes in the various reservoirs plus the total ^{14}C decay.

Fig. 4 shows the reconstructed ^{14}C production rate inferred from the measured ^{14}C concentrations in tree rings. The black lines show the ^{14}C production reconstructed using the OD carbon cycle model by Siegenthaler (1983). The grey bands indicate the $1-\sigma$ errors inferred from the Monte-Carlo calculations. The comparison with the results from the three different models (panel b and c) illustrates that model dependencies are relatively small. The data are shown after low-pass filtering with cut-off frequencies of 1/20 and 1/50 yr^{-1}. Biosphere and oceanic ventilation are included in a different way in the HILDA model compared to the OD model, which results in only slightly different amplitudes of the ^{14}C production rate. The different methods to include hemispheric $\Delta^{14}C$ do not yield significant differences in the results. Results obtained with the three models also agree well over the industrial period.

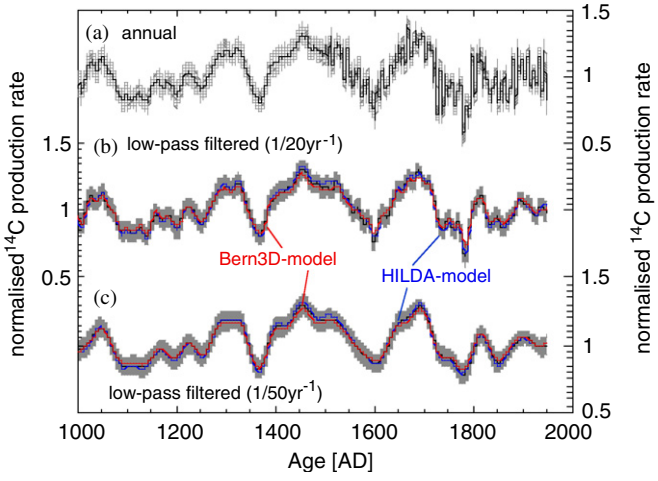

Fig. 4. Reconstructed ^{14}C production rate based on the $\Delta^{14}C$ record. Panel a shows the ^{14}C production rate calculated from the low-pass filtered $\Delta^{14}C$ record with the Outcrop-diffusion model (cut-off frequency: 1/8 yr^{-1}). Panel b and c show the comparison of the reconstructed ^{14}C production using the OD (black curve), the HILDA (blue curve) and the Bern3D carbon cycle model including the southern hemisphere data (red curve) after removing short-term changes on time scales shorter than 20 (b) and 50 (c) years. The $1-\sigma$ errors are based on 100 Monte-Carlo simulations, which include the errors in the $\Delta^{14}C$ data.

4.3. Solar modulation function inferred from $\Delta^{14}C$

By combining the results of the ^{14}C production calculations (Fig. 1), the geomagnetic field intensity changes (Fig. 2) and the reconstruction of the ^{14}C production rate (Fig. 4) it is possible to infer the past changes in the solar modulation function. As indicated by our results, the relative changes in radiocarbon production rates can be calculated relatively accurately. However, there are uncertainties in the absolute amount of radiocarbon production and in the link between the absolute numbers of the ^{14}C production rate and solar modulation. These uncertainties would hamper the accuracy of directly inferred values of the solar modulation function. Hence, we pursue a different strategy and link the radiocarbon-based solar modulation record to independently derived records of solar modulation from neutron monitor, balloon-borne and ionisation chamber measurements available for the last approximately 70 yr.

Neutron monitor data provide good estimates for past changes in the cosmic ray flux entering the Earth's atmosphere (Fig. 5). Masarik and Beer (1999) reconstructed the changes in Φ for the period from 1953 to 1995 AD using the data from the neutron monitor at Climax, CO. The neutron monitor data can be extended to 1937 AD by using ionisation chamber data from Cheltenham (Beer, 2000). Since the Cheltenham ionisation chamber data could include uncontrollable drifts (McCracken, personal information) McCracken and Heikkila (2003) suggested an alternative reconstruction of the cosmic ray flux before 1953 AD. It is based on balloon-borne measurements by Neher and shows a lower solar magnetic modulation before 1950 AD (McCracken and Heikkila, 2003). We show an updated version of this record in Fig. 5 that includes the non-linear relationship between the balloon-borne measurements and the climax neutron monitor measurements (McCracken, personal information). The ionisation chamber and balloon-borne records were connected to the Climax data by normalizing the data to obtain the same average value and the same standard deviation as the Climax record for the period of overlap.

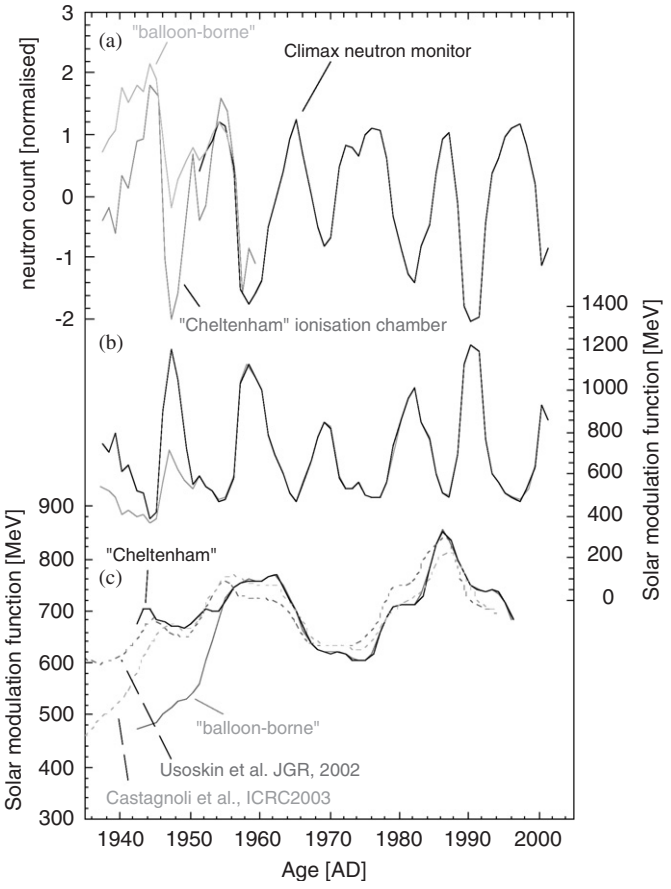

Fig. 5. Solar modulation from 1937 to 2000 AD inferred from neutron monitor data from Climax, Colorado, ionisation chamber data from Cheltenham and balloon-borne ionisation measurements. Panel a shows the Climax neutron monitor data (black), the Cheltenham data (Beer, 2000) (dark grey) and the balloon-borne measurements (McCracken and Heikkila, 2003; updated version, McCracken personal communication) (light grey). The Cheltenham and balloon-borne data were normalised to obtain agreement between average value and standard deviation with the Climax data in the time periods of overlap. The solar modulation (b) is based on neutron monitor data (Masarik and Beer, 1999), which was extended using the Cheltenham (black) and balloon-borne (grey) data. Panel (c) shows the comparison with independent estimates of solar modulation based on the sunspot record (dashed lines, 11-yr running averages) (Solanki et al., 2000; Usoskin et al., 2002; Cini Castagnoli et al., 2003). The sunspot-based records were normalised to obtain agreement between the different estimates for the period from 1954 to 1994 AD.

The relation between neutron monitor data and Φ as proposed by Masarik and Beer (1999) was fitted with an exponential function. It is then possible to extend the reconstructions of Φ back to 1937 AD by applying this exponential relationship to the extended neutron monitor record. The two reconstructions shown in Fig. 5b provide estimates of variations in Φ that can be connected to the ^{14}C-based reconstruction of solar activity before 1950 AD.

The differences between the two reconstructions of the solar modulation function before 1950 AD are relatively large. While the ionisation chamber data show no strong change before 1950 AD the data from balloon-borne measurements indicate a lower solar activity during the 1940s especially during the two solar maximums. Even though not perfect, the balloon-borne measurements are considered to be more reliable since differences among three different independent ground-based ionisation chamber records indicate different trends (McCracken, personal information). In Fig. 5c we compare these solar modulation estimates with two independent reconstructions of the solar modulation function before 1950 AD (Cini Castagnoli et al., 2003; Usoskin et al., 2002). These are based on a conversion of the sunspot record to an estimate of the solar magnetic field (Solanki et al., 2000). If the model of Solanki et al. (2000) is correct around 1950 AD this comparison indicates that the Cheltenham data overestimate and the Neher data underestimate the solar modulation before 1950 AD. We therefore suggest that these two records represent upper and lower estimates for changes in Φ before 1950 AD. Comparing the 11-yr averages from 1942 to 1954 AD the comparison in Fig. 5c shows that the Cheltenham-based data overestimates the Φ changes by approximately 4% (Usoskin et al., 2002) and 9% (Cini Castagnoli et al., 2003) and that balloon-based data underestimate the Φ changes by approximately 25% (Usoskin et al., 2002) and 19% (Cini Castagnoli et al., 2003). This comparison might suggest that the Cheltenham ionisation chamber data set is a better measure for the solar activity before 1950 AD. However, there are contradictions between the model results of Solanki et al. (2004) and the ^{14}C-based estimate of the solar magnetic modulation during the last 400 yr (Muscheler et al., 2005b). Therefore, we will apply in the following both estimates of solar magnetic modulation shown in Fig. 5b to normalise our records and consider these two estimates as upper and lower limits for the normalisation of the ^{14}C production rate record.

Fig. 6 shows the changes in the solar modulation function inferred from the ^{14}C production rate. The annual ^{14}C production rate record was normalised to obtain the same average Φ values for the neutron monitor and ^{14}C-based data from 1937 to 1950 AD. The ^{14}C production rate inferred from decadal data (3D model) was normalised to obtain the same average value from 1939 to 1949 AD (11-yr average). This shorter period was selected instead of the 1937–1950 AD period to avoid a potential artefact by including two solar maximums and only one solar minimum in the normalisation. The use of different records to extend Φ to 1937 AD has consequences for the normalisation of the radiocarbon production record. Fig. 6a shows the normalisation based on the Cheltenham ionisation chamber data and Fig. 6b the results according to the balloon-borne data. The balloon-borne data suggest a strong change before 1950 AD which means that the Δ^{14}C-based solar modulation curve is, on average, shifted by approximately 200 MeV to lower values. The curves are calculated from the ^{14}C production rate by using the geomagnetic field reconstruction of Yang et al. (2000) and Korte and Constable (2005) (see Fig. 2). The northern hemisphere Δ^{14}C record clearly exhibits the 11-yr cycle for the period where the record is based on the annual Δ^{14}C

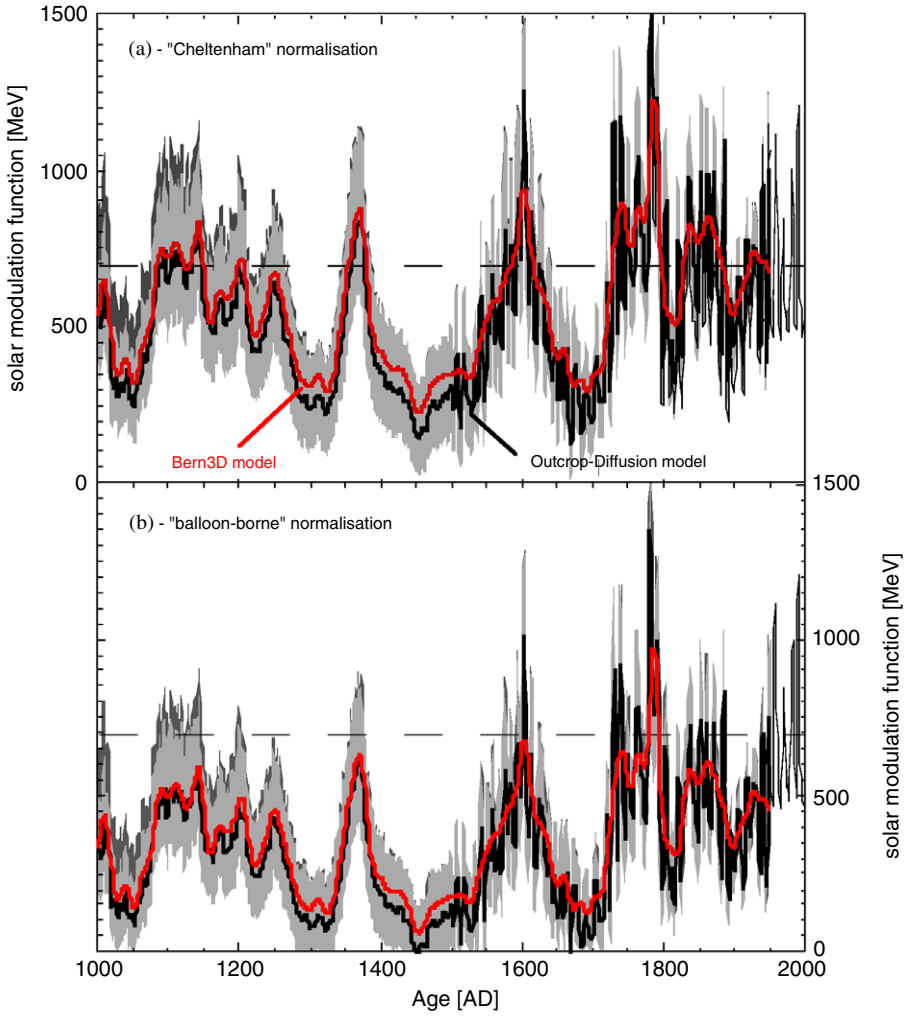

Fig. 6. Variations in the solar modulation function Φ inferred from the ^{14}C production rate and the ionisation chamber data from Cheltenham (Beer, 2000) (a) and the alternative normalisation based on the balloon-borne data (McCracken and Heikkila, 2003) (b). We normalised the data to obtain agreement between the average values of Φ in the overlapping period. The light grey band shows the error calculated from the $\Delta^{14}C$ and archeomagnetic field errors. The dark grey band shows the error calculation using the $\Delta^{14}C$ data and the alternative estimate of global geomagnetic dipole moment (Korte and Constable, 2005). The red lines show the results based on the Bern3D model results. The dashed line shows the level of the average solar magnetic modulation from 1950 to 2000 AD of approximately 700 MeV.

data and Φ varied between 0 and 1500 MeV during the last 1000 yr. The solar modulation records indicate that the solar magnetic shielding was relatively high during the last 50 yr. Nevertheless, during the last 1000 yr there were periods with a similar or even higher level of solar modulation compared to today's values. The period around 1780 AD, which follows the Maunder minimum, shows an especially strong increase in solar modulation. Fig. 6 shows that solar activity has varied rhythmically with a period of approximately 200 yr during the last 1000 yr. The solar modulation calculated with the Bern3D model indicates very similar solar magnetic modulation as the calculations based on the OD model. Therefore, the approach to average the northern and southern hemisphere $\Delta^{14}C$ data yields similar results as to spatially resolve the atmospheric $\Delta^{14}C$ records in the 3D model.

Due to the generally lower geomagnetic field intensities during the last 1000 yr, the calculations using Korte and Constable's (2005) record result in a higher solar modulation function during the last 1000 yr than the results based on Yang et al. (2000). However, due to the large error bars of Yang et al. (2000) the results usually agree within the errors.

This reconstruction of solar magnetic activity in the past includes two main uncertainties. First, the normalisation of the ^{14}C production record was based on a relatively short period of overlap between ^{14}C and neutron monitor records (roughly one solar 11-yr cycle). Nevertheless, as mentioned the two estimates shown in Figs. 6a and b show the two extreme cases. The Cheltenham ionisation chamber data (Fig. 6a) show almost no change in the 11-yr averaged solar modulation before 1950 AD while the balloon-borne measurements indicates a very strong change before 1950 AD. The latter normalisation leads to values of Φ which are often close to 0 MeV, which represents the lowest physically meaningful limit.

The second uncertainty is that the ^{14}C record might be influenced by changes in the carbon cycle. In the next section we will investigate the various ^{10}Be records from ice cores as these provide complementary information on past changes in solar activity since ^{10}Be is, unlike ^{14}C, not influenced by the carbon cycle.

5. The interpretation of ^{10}Be records in terms of radionuclide production

5.1. The data

As mentioned ^{10}Be records could be influenced by changes in atmospheric circulation and deposition. Our approach is to include ^{10}Be data from different locations to reduce such local influences by averaging the data. Fig. 7 shows the ^{10}Be data that was used for the following analysis. We used the published ^{10}Be records that have an average time resolution in the order of 20 yr or better and that cover at least 500 of the last 1000 yr. There are two ^{10}Be ice core records from Antarctica that match these criteria. They are from the South Pole (Raisbeck et al., 1990) and from Dome Concordia (Dome C) (Beer et al., 1991). These data can be combined with four records from Greenland measured in the Milcent (Beer et al., 1991), Camp Century (Beer et al., 1988), GRIP (Yiou et al., 1997; Muscheler et al., 2004b) and Dye3 (Beer et al., 1990) ice cores. Since the records cover different time periods and different average deposition levels, we normalised them relative to the geomagnetic field record. We assume that the time-averaged ^{10}Be concentration of a particular record corresponds to the time-averaged ^{10}Be production rate as calculated from the geomagnetic field intensity over the time period spanned by the ^{10}Be record and an average solar modulation. This allows us to compare and combine the different ^{10}Be records. However, this method requires relatively long ^{10}Be records to ensure that we do not remove solar induced ^{10}Be changes in the averaging procedure. For example, if a ^{10}Be record only covered the period of the Maunder minimum we basically would remove the solar-induced increase in ^{10}Be by the normalisation to the geomagnetic field record. Since all the ^{10}Be records in Fig. 7 cover more than 500 yr such a bias is unlikely to affect centennial variations, but the normalisation could potentially bias millennial scale changes in the inferred solar modulation. Comparison between ^{10}Be and ^{14}C production records indicate that the ice core time scales can have errors of up to 20 yr, but in most cases the dating errors are smaller. This can cause additional uncertainties in the shorter-term variations ($T<20$ yr) but not in the longer-term changes.

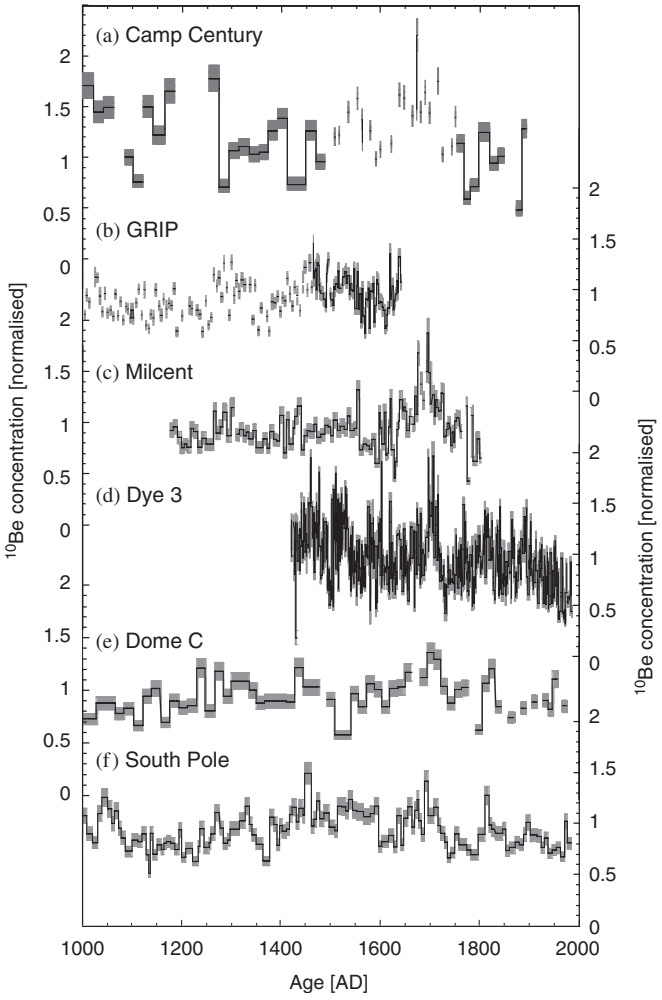

Fig. 7. Normalised ^{10}Be concentrations measured in ice cores from Greenland and Antarctica. Panel a shows data from Camp Century (Beer et al., 1988), panel b from GRIP (Muscheler et al., 2004b; Yiou et al., 1997), panel c from Milcent (Beer et al., 1991), panel d from Dye3 (Beer et al., 1990), panel e from Dome Concordia (Beer et al., 1991) and panel f from the South Pole (Raisbeck et al., 1990). $1-\sigma$ errors are indicated in grey.

Fig. 8 shows the combined ^{10}Be data including errors of the mean values ($1-\sigma$) and the periods to which the individual cores contribute. As mentioned, due to potential errors in ice core time scales and due to the different time resolution of the ^{10}Be records, it is not possible to study the high-resolution changes with the composite ^{10}Be record. The following calculations are based on the low-pass filtered ^{10}Be record ($v_{cutoff} = 1/20\,yr^{-1}$; red curve in Fig. 8). The blue line in Fig. 8 shows an average ^{10}Be record (low-pass filtered $v_{cutoff} = 1/20\,yr^{-1}$) where we, at each point in time, removed one data point that showed the largest difference to the average ^{10}Be curve (if more than two records entered the averaging procedure; later referred to as "reduced" ^{10}Be record). It shows that, in most cases, individual curves do not dominate the average record.

5.2. Solar modulation inferred from the ^{10}Be record

To calculate the solar modulation from the ^{10}Be record we again apply the production calculations by Masarik and Beer (1999) and the geomagnetic field records shown in Fig. 2. Since the change in the averaged ^{10}Be record is relatively strong for the last 100 yr we cannot apply the normalisation based on the neutron monitor data. Such an

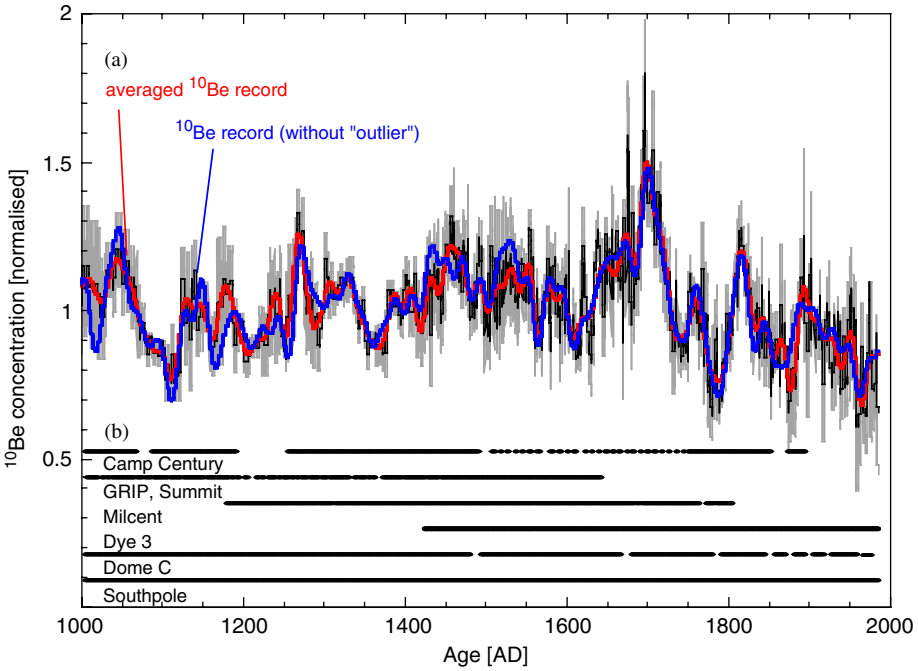

Fig. 8. Averaged ^{10}Be concentration and the cores on which the averaged values are based on. The black curve in panel a shows the averaged values including the standard deviations of the mean values. The red curve shows the low-pass filtered ^{10}Be concentration ($\nu_{cutoff} = 1/20\,yr^{-1}$). Panel b shows to which periods the individual cores contribute to the average ^{10}Be record. The blue curve show the low-pass filtered ^{10}Be concentration ($\nu_{cutoff} = 1/20\,yr^{-1}$) where we, at each point in time, removed one value from the averaging procedure that had the strongest disagreement with the mean.

approach would yield negative values of Φ for several periods of low solar activity during the last 1000 yr which points to a residual climatic signal in the averaged ^{10}Be record for the second part of the 20th century (remark: second part of the 20th century refers to the period 1950–1985 AD since none of the ^{10}Be records extends to today). Thus we normalised the ^{10}Be record according to the ^{14}C-based Φ reconstruction to obtain agreement between the average ^{10}Be- and ^{14}C-based values for Φ for the period from 1000 to 1850 AD. This was done for calculations normalised on the balloon-borne measurements (Fig. 6b). The changes in the solar modulation function are based on the average ^{10}Be records shown in Fig. 8. The black curve in Fig. 9a shows the solar modulation including the full ^{10}Be record and the geomagnetic field record by Yang et al. (2000). The grey band includes the geomagnetic field errors and the errors of the average ^{10}Be record. The red curve shows a slightly higher solar modulation caused by the lower geomagnetic field intensity suggested by Korte and Constable (2005). The blue curve shows the solar modulation of the reduced ^{10}Be record shown in Fig. 8.

Field et al. (2006) suggested that ^{10}Be from polar regions should show an approximately 20% enhancement of the solar induced production variations compared to the global average. Similarly according to their model results the geomagnetic field intensity signal should be slightly dampened by 20% in ^{10}Be records from polar regions. Considering the absent geomagnetic modulation in the ^{10}Be production rate over the geomagnetic poles this still means that the atmospheric circulation mixes ^{10}Be relatively well in the atmosphere. Consequently, the solar modulation function inferred from ^{10}Be based on such a mixing scheme is not very different from the results based on the initial assumption of a globally well-mixed ^{10}Be signal. Fig. 9b shows the consequences for the modulation function. If we assume that ^{10}Be shows such a polar-biased signal the amplitude of the solar modulation becomes smaller. However, the differences are still within the error band indicated in Fig. 9a.

Our combined ^{10}Be record shows the highest values during the second half of the 20th century (around 1960 AD). These high values are caused by the strong decrease of the Dye3 ^{10}Be data which led Usoskin et al. (2003) to their conclusions about the record high solar activity. This feature is dampened by the procedure used to remove "outliers", which results in the reconstruction that shows that the last 50 yr of solar modulation are high but not exceptionally high with respect to the last 1000 yr.

6. Comparison of ^{10}Be- and ^{14}C-based solar modulation records

In general, the comparison of ^{10}Be- and ^{14}C-based solar modulation function indicates a good agreement (Fig. 10). For this comparison both records were low-pass filtered at a cut-off frequency of $1/20\,yr^{-1}$. The curves show the data according to the normalisation based on the balloon-borne data. The agreement between the two records confirms that carbon cycle changes do not significantly influence the

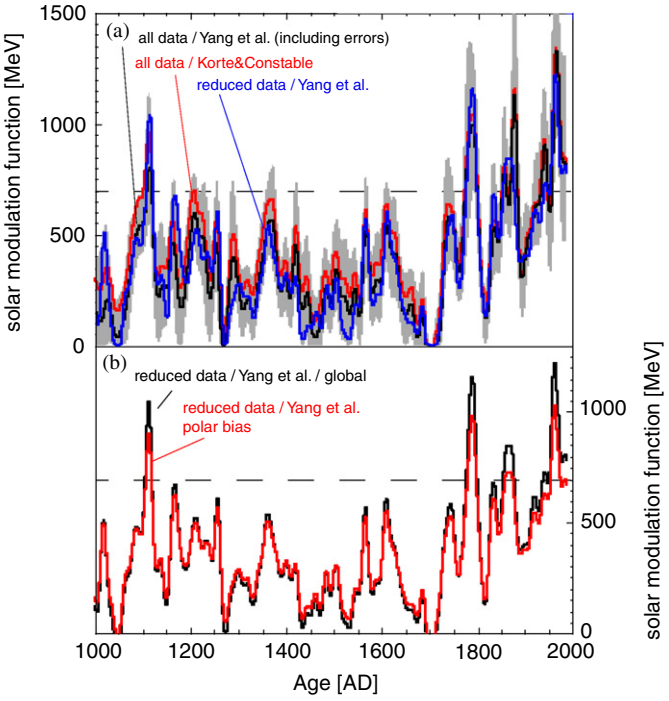

Fig. 9. Changes in the solar modulation function during the last 1000 yr inferred from the ^{10}Be records. The black curve in panel a is calculated from the low-pass filtered ^{10}Be concentration ($\nu_{cutoff} = 1/20\,yr^{-1}$) including all ^{10}Be data. The grey band shows the $1-\sigma$ errors that are based on the uncertainties in the averaged ^{10}Be record and the geomagnetic field. The red curve shows the solar modulation based on the averaged ^{10}Be record and the alternative estimate for the global geomagnetic dipole moment (Korte and Constable, 2005). The blue curve is calculated from the reduced ^{10}Be average (blue curve in Fig. 8) using the Yang et al. geomagnetic field data. Panel b shows the differences between the assumption that the average ^{10}Be record shows global changes and if we include the results of Field et al. that suggest that ^{10}Be in polar regions shows a 20% enhancement in solar-induced variability.

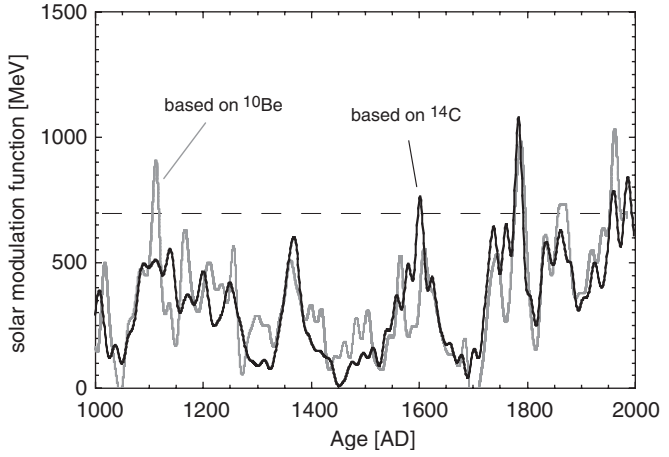

Fig. 10. Comparison of the solar modulation function based on ^{10}Be (grey curve) and ^{14}C (black curve). Both curves show the solar modulation function after low-pass filtering at a cut-off frequency of $1/20\,yr^{-1}$. The curves are obtained by normalisation to the balloon-borne data and geomagnetic field intensity indicated by Yang et al. (2000). We show the ^{10}Be record without the "outliers".

atmospheric ^{14}C concentration and that the averaging of the various ^{10}Be records provides a good estimate of the global changes in the ^{10}Be production rates. There are, however, differences. For example, the ^{10}Be-based solar modulation exhibits stronger short-term variations than the solar modulation record inferred from ^{14}C. The larger short-term variations are already visible in some of the individual ^{10}Be records shown in Fig. 7. They could be due to local changes in ^{10}Be transport and deposition. For example, the record from Camp Century shows some disagreement with other ^{10}Be records. In addition, the incomplete time coverage or dating uncertainties of some of the records can add short-term variability to the averaged record. Since we removed only one "outlier" at each point in time we did not remove all of the differences between the records for our average curve. By using the reduced ^{10}Be record and the "transport" corrections suggested by Field et al. (2006) we improve the agreement between our ^{14}C and ^{10}Be records. If we include the full ^{10}Be record we obtain a relatively strong increase in solar activity (due to the Dye3 record) that is not present in the combined ^{14}C and neutron monitor data set. The comparison with the ^{14}C-based record suggests that we can improve the ^{10}Be-based record by removing outliers and by assuming that the ^{10}Be record shows a slight enhancement of the solar induced ^{10}Be changes.

In the perspective of the observed global climate warming of the 20th century it is important to study the changes in solar activity during the last 150 yr. In the following we investigate in more detail the different ^{10}Be records during this period. The ^{10}Be concentrations measured in the Greenland Dye3 ice core indicate high values of solar activity during the second part of the 20th century (Beer et al., 1990). By contrast, the ^{10}Be concentrations measured in the ice core from the South Pole do not show this trend (Raisbeck and Yiou, 2004). The question is, therefore, how reliable is the averaged ^{10}Be record for this period when it is based on ^{10}Be records that disagree? Additional ^{10}Be records for the last century confirm the discrepancy between the Greenland and Antarctic ^{10}Be data. Unpublished data from the Greenland GISP2 ice core seem to agree with the Greenland Dye3 ^{10}Be record (K. Nishizumii, personal information). Furthermore, unpublished ^{10}Be data from a shallow core obtained at Summit, Greenland also point to a stronger decrease in ^{10}Be deposition than indicated by the record from the South Pole. The record from Dome C rather agrees with the data from the South Pole. Raisbeck and Yiou (2004) mention that this is supported by new data from Dome C. To summarize, there are three records from Greenland that show a relatively strong decrease in ^{10}Be deposition during the second part of the 20th century. Three records from Antarctica do not show this decrease. This difference suggests that the ^{10}Be concentration in at least one of these regions is influenced by changes in ^{10}Be transport and deposition. It could well be that the climate change during the second part of the 20th century

influenced the ^{10}Be deposition in Greenland and/or in Antarctica. The observed climate changes in the northern hemisphere have been considerably larger than in the southern hemisphere during the last century. The general warming with increased hydrologic activity is consistent with more snow, less aerosols and consequently reduced ^{10}Be concentrations. Therefore, it seems likely that ^{10}Be measurements in Greenland contain climate artefacts. This is partly confirmed by our method to remove "outliers" in the averaged curve. Part of the ^{10}Be data from Dye3 is removed by this procedure during the second part of the 20th century and we obtain a better agreement with the combined neutron and ^{14}C record (see Fig. 10). Nevertheless, the reconstruction of past changes in solar activity using ^{10}Be records for the last century will remain problematic as long as the causes of these differences are not understood.

In the following section we compare our radionuclide-based estimate of solar modulation with alternative estimates of solar activity. Unless stated otherwise, we will use our most likely estimates of solar modulation. These are based on the globally averaged Δ^{14}C data normalized to the balloon-borne estimate of solar modulation from 1937 to 1950 AD. We include the Yang et al. geomagnetic field record since it encompasses the Korte and Constable geomagnetic field estimate for most of the investigated periods. This could mean that our average value for solar modulation is generally slightly too low further back in time. In addition, we include the ^{10}Be data where we removed one "outlier" at each point in time and that we normalised to the ^{14}C record shown in Fig. 10. Again, we use the Yang et al. geomagnetic field record for this calculation.

7. Comparison with the sunspot records

More than 150 yr ago Rudolf Wolf started to systematically reconstruct the past changes in sunspot number. Hoyt and Schatten (1998) proposed an improved record to estimate the past changes in sunspot number, the so-called group sunspot number. The Wolf sunspot number and the group sunspot number agree well for the last 100 yr but the group sunspot number indicates lower solar activity before that period (Fig. 11a) (Hoyt and Schatten, 1998). The sunspot numbers are connected to the magnetic activity on the Sun's surface, which is assumed to correlate with the open magnetic flux (Solanki et al., 2000). Therefore, according to this model a close relationship between sunspot numbers and ^{10}Be and ^{14}C records is expected.

Fig. 11b shows the comparison of our ^{14}C-based reconstruction of the solar modulation function and the group sunspot number. As already pointed out by Stuiver and Braziunas (1993) there is a high agreement of the changes in the ^{14}C production rate and changes in sunspots number associated with the solar 11-yr cycle. This comparison also shows that the 11-yr cycle continued

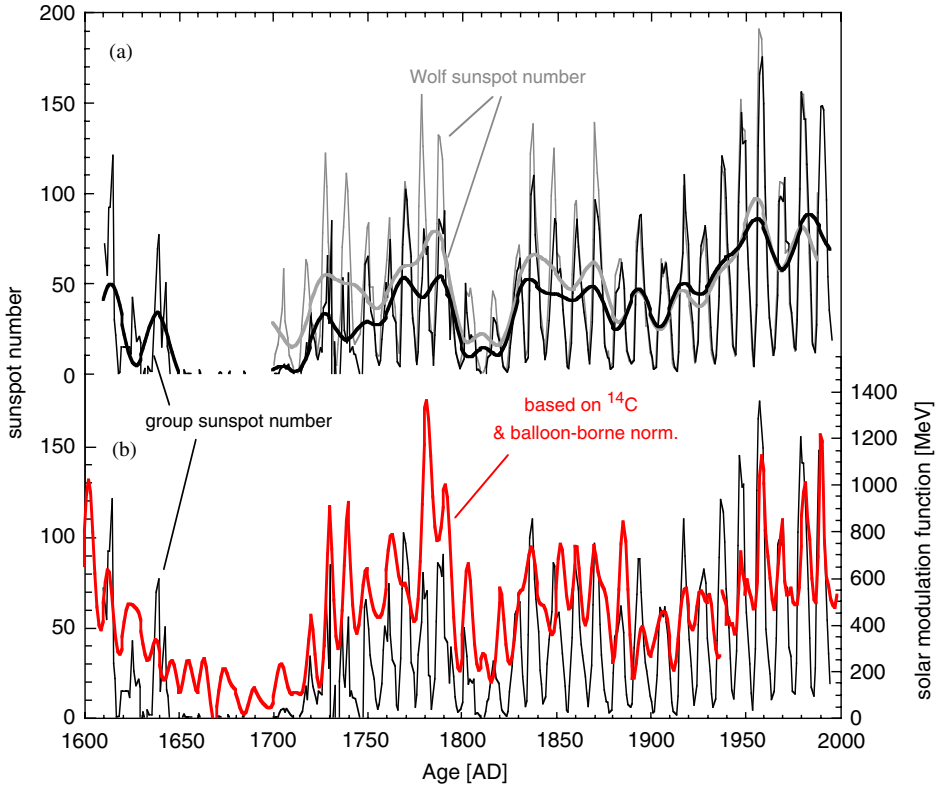

Fig. 11. Comparison of sunspot number records with ^{14}C-based changes in the solar modulation function. Panel a shows the Wolf and the group sunspot number. The smoothed lines show the low-pass filtered (1/20 yr^{-1}) data. Panel b shows the comparison of the ^{14}C and neutron monitor-based (balloon-borne data) solar modulation function with the group sunspot number.

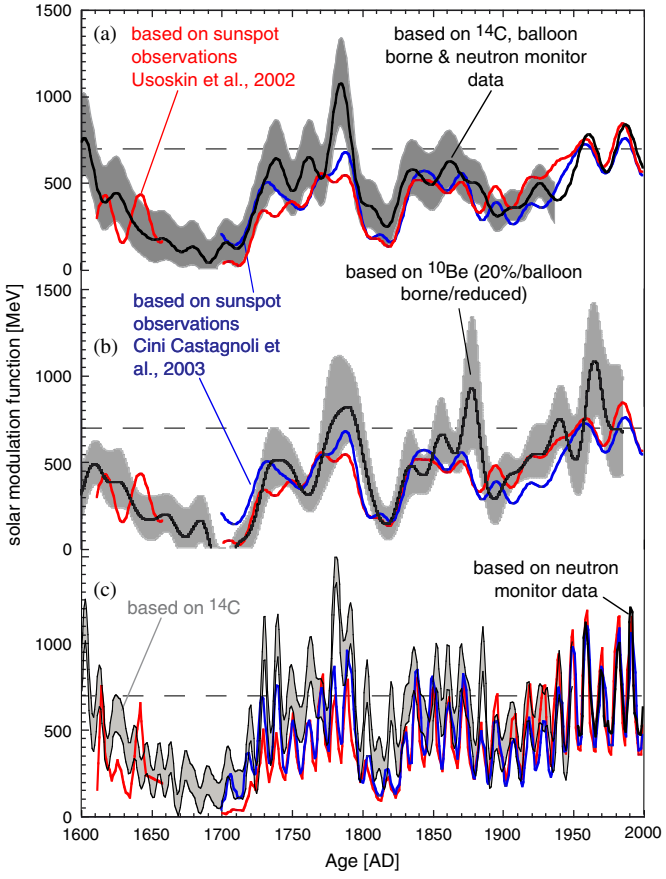

Fig. 12. Comparison of different estimates of the solar modulation function for the last 400 yr. The red and blue lines are Φ estimates inferred from the sunspot record (Cini Castagnoli et al., 2003; Solanki et al., 2000; Usoskin et al., 2002) (low-pass filtered at $1/20\,yr^{-1}$). Panel a shows the comparison with the ^{14}C-based record normalised to the balloon-borne and neutron monitor data. Panel b shows the comparison with the solar magnetic modulation inferred from the averaged ^{10}Be record. Panel c shows the comparison of sunspot-based records and the two average solar magnetic modulation curves inferred from the two methods to normalise the ^{14}C data (see text) without filtering the data and without including other errors.

during the Maunder minimum where almost no sunspots were observed. The ^{10}Be record from Dye3 also indicates that this solar modulation continued through the Maunder minimum (Beer et al., 1998). Fig. 11b suggests that solar activity must exceed a solar modulation of 250 MeV to produce observable sunspots on the Sun's surface. This solar modulation estimate agrees well with independent results for solar minimum periods inferred from ^{10}Be records by McCracken et al. (2004). Fig. 11 compares sunspots directly with the solar modulation function and it is clear that these two quantities are not linearly related. In the following we compare solar modulation estimates based on the sunspot record with ^{14}C and ^{10}Be-based reconstructions. Cini Castagnoli et al. (2003) and Usoskin et al. (2002) reconstructed the solar modulation using a model to convert the sunspot number into an estimate of the Sun's large scale magnetic field (Solanki et al., 2000). The differences between the two reconstructions (Fig. 12) resemble the differences between Wolf and group sunspot number. Fig. 12a compares these records to the ^{14}C-based solar modulation using the "balloon-borne" normalisation. All curves show the variations on time scales longer than 20 yr. Fig. 12b shows the same comparison with the ^{10}Be-based solar modulation record. Fig. 12c shows this comparison for the annual values. It shows that the short-term changes agree well. Nevertheless, there are differences around 1780 AD where the ^{14}C-based reconstruction suggests higher solar modulation than the sunspot-based record.

The solar modulation maximum around 1780 AD indicated by the ^{14}C and ^{10}Be data was on the level of the second part of the 20th century or even higher. It is noteworthy that especially during this period the sunspot record is relatively uncertain (Hoyt and Schatten, 1998) even if this probably cannot completely explain the differences between the records. The disagreement around 1780 AD between sunspot and cosmogenic radionuclide records shows that it is not straightforward to convert one record into the other (Muscheler et al., 2005b). Another indication for a more complicated relationship between sunspots and radionuclide production is the presence of solar modulation in the 11-yr band in the tree-ring ^{14}C and the Dye3 ^{10}Be record during the Maunder minimum when almost no sunspots were observed (Beer et al., 1998).

8. Comparison with irradiance estimates

According to sunspot and cosmogenic radionuclide records the Sun was in a phase of relatively high activity during the last 25 yr of direct solar satellite observations. Therefore, the solar irradiance during the Maunder minimum lies outside the range of calibration. The question if the relatively long Maunder minimum is comparable in irradiance to each solar minimum during an 11-yr cycle is not yet doubtlessly solved. If all solar phases with no sunspots were identical to each other the irradiance changes from the Maunder minimum to today would only be very small (in the order of 1‰). However, during "modern" solar minima the annually averaged sunspot numbers do not reach values of zero and also the cosmogenic radionuclide records indicate that, for example, the Maunder minimum significantly differs from a solar minimum during an 11-yr cycle. In contrast to the sunspot number the cosmogenic radionuclide production rate does not always reach a similar level during each solar minimum. This could indicate that irradiance reconstructions based on the sunspot record might be unsuitable to capture the complete range of solar variability. In addition, irradiance changes are not only determined by darkening effects of sunspots but also by the bright areas (faculae) around them.

There are two records of past changes in solar irradiance widely used in climate modelling (Bard et al., 2000; Lean et al., 1995). Lean et al. (1995) reconstruction is based on the group sunspot record scaled with an estimate for the

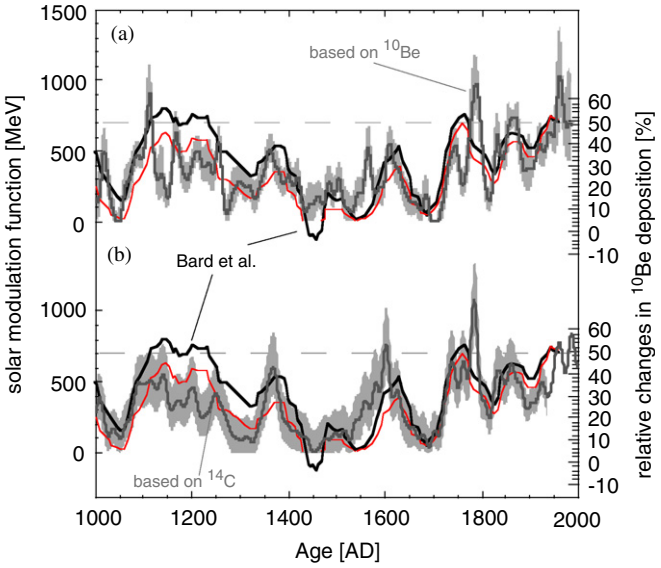

Fig. 13. Comparison of the South Pole ^{10}Be record (on which Bard et al. (2000) based their reconstruction of solar irradiance) and ^{14}C and composite ^{10}Be-based solar magnetic modulation records. Panel a shows the comparison of ^{10}Be-based solar magnetic modulation with ^{10}Be concentration from the South Pole. Panel b shows the comparison with the ^{14}C-based record. The red curves show the solar modulation function inferred from the ^{10}Be record from the South Pole under the assumption that this record reflects the global changes in ^{10}Be production rate. The curves are obtained using the geomagnetic field reconstruction from the archaeomagnetic data and the normalisation to the balloon-borne solar modulation estimates.

solar irradiance during the Maunder minimum. Therefore, Lean et al.'s record exhibits similar differences to the cosmogenic radionuclide records as shown in Fig. 11. Bard et al. (2000) based their reconstruction on the measured ^{10}Be concentration from the South Pole (see Fig. 7f) with different scaling factors for solar irradiance during the Maunder minimum. Fig. 13 depicts the ^{10}Be record from the South Pole that Bard et al. (2000) linearly related to changes in solar irradiance. Since the functional dependency between irradiance and solar magnetic modulation is not yet clear we only compare the cosmogenic radionuclide records to illustrate the periods during which the irradiance reconstruction based on the South Pole data exhibits differences to our ^{10}Be and ^{14}C-based solar modulation records. The axes are scaled to obtain agreement between the records for the Maunder minimum and for the first 50 yr in the 20th century. One reason for differences between our estimates for Φ and Bard et al.'s reconstruction is that they did not correct for the geomagnetic influence. Nevertheless, Field et al. (2006) suggest that the geomagnetic field does influence the ^{10}Be deposition rate in polar regions and, therefore, any changes in it have to be included in these calculations. Partly due to the absence of a geomagnetic field correction Bard et al. (2000) infer relatively high solar activity around 1200 AD compared to our ^{10}Be and ^{14}C-based records. The very low solar activity values around 1450 and 1550 AD as indicated by Bard et al. are less prominent in the composite ^{10}Be and the ^{14}C-based solar activity records. In contrast to Bard et al. these records indicate that solar activity during the Spörer minimum around 1500 AD was comparable to the Maunder minimum. The solar activity maximum around 1780 AD is present in both ^{14}C and ^{10}Be-based reconstructions of solar activity but it is less prominent in Bard et al.'s reconstruction of irradiance. The red curves in Fig. 13 shows the solar modulation function based on the ^{10}Be record from the South Pole. It illustrates the non-linear relationship between ^{10}Be production and solar magnetic modulation and it also shows that a geomagnetic correction has a significant influence on the reconstructed long-term changes in solar activity. All curves in Fig. 13 are calculated using the geomagnetic field reconstruction by Yang et al. (2000) and the normalisation is based on the extension of the neutron monitor record using the balloon-borne data.

9. Conclusions

By considering various cosmogenic radionuclide records we have calculated two records of changes in the solar modulation function over the last 1000 yr. Six different ^{10}Be records from ice cores from Greenland and Antarctica are used to calculate a ^{10}Be-based history of solar modulation. The comparison of the individual records indicates that at least some of the ^{10}Be records are influenced by local changes in atmospheric transport and deposition but, nevertheless, all records show the major changes in solar activity. The differences between the ^{10}Be records from Greenland and Antarctica for the period after 1950 AD have led to strongly differing conclusions about solar activity in the past (Bard et al., 2000; Usoskin et al., 2003). While the records from Greenland indicate a relatively low ^{10}Be production after 1950 AD this trend is rather opposite in the Antarctic records. The 11-yr averages of the neutron monitor and sunspot data show a relatively stable solar activity during the second part of the 20th century.

We get good agreement with independent solar modulation estimates inferred from tree-ring Δ^{14}C measurements. Natural carbon cycle changes are not expected to significantly influence the Δ^{14}C records and we can reliably include the Suess effect in our calculations of the ^{14}C production rate. The main uncertainties are due to the normalisation of the record and the geomagnetic field changes.

Regardless of these uncertainties, the cosmogenic radionuclide records indicate that the current solar activity is relatively high compared to the period before 1950 AD. However, as the mean value during the last 55 yr was reached or exceeded several times during the past 1000 yr the current level of solar activity can be regarded as relatively common.

Acknowledgements

Comments by Robert Delmas and two anonymous reviewers helped to significantly improve this manuscript. We would like to thank Ken McCracken for very helpful discussions and for providing unpublished data. We would also like to thank Monika Korte for providing model results. Ann-Marie Berggren provided helpful corrections. The neutron data were provided by the University of Chicago (National Science Foundation Grant ATM-9613963). This work was supported by the Swiss National Science Foundation, NSF and NASA.

References

Bard, E., Raisbeck, G.M., Yiou, F., Jouzel, J., 2000. Solar irradiance during the last 1200 years based on cosmogenic nuclides. Tellus 52B, 985–992.

Beer, J., 2000. Neutron monitor records in broader historical context. Space Science Reviews 93, 107–119.

Beer, J., Siegenthaler, U., Bonani, G., Finkel, R.C., Oeschger, H., Suter, M., Wölfli, W., 1988. Information on past solar activity and geomagnetism from ^{10}Be in the Camp Century ice core. Nature 331, 675–679.

Beer, J., Blinov, A., Bonani, G., Finkel, R.C., Hofmann, H.J., Lehmann, B., Oeschger, H., Sigg, A., Schwander, J., Staffelbach, T., Stauffer, B., Suter, M., Wölfli, W., 1990. Use of ^{10}Be in polar ice to trace the 11-year cycle of solar activity. Nature 347, 164–166.

Beer, J., Raisbeck, G.M., Yiou, F., 1991. Time variations of ^{10}Be and solar activity. In: Sonett, C.P., Giampapa, M.S., Matthews, M.S. (Eds.), Time Variations of ^{10}Be and Solar Activity. University of Arizona press, Tucson, pp. 343–359.

Beer, J., Tobias, S.M., Weiss, N.O., 1998. An active sun throughout the maunder minimum. Solar Physics 181, 237–249.

Bond, G., Kromer, B., Beer, J., Muscheler, R., Evans, M.N., Showers, W., Hoffmann, S., Lotti-Bond, R., Hajdas, I., Bonani, G., 2001. Persistent solar influence on North Atlantic climate during the Holocene. Science 294, 2130–2136.

Bruno, M., Joos, F., 1997. Terrestrial carbon storage during the past 200 years: a Monte Carlo analysis of CO_2 data from ice core and atmospheric measurements. Global Biogeochemical Cycles 11, 111–124.

Caballero-Lopez, R.A., Moraal, H., 2004. Limitations of the force field equation to describe cosmic ray modulation. Journal of Geophysical Research 109, A01101.

Cini Castagnoli, G.C., Lal, D., 1980. Solar modulation effects in terrestrial production of Carbon-14. Radiocarbon 22, 133–158.

Cini Castagnoli, G.C., Cane, D., Taricco, C., Bhandari, N., 2003. GCR flux decline during the last three centuries: extraterrestrial and terrestrial evidences. In: Kajita, T., Asaoka, Y., Kawachi, A., Matsubara, Y., Sasaki, M. (Eds.), GCR Flux Decline during the last Three Centuries: Extraterrestrial and Terrestrial Evidences. Universal Academy Press, Inc., pp. 4045–4048.

Denton, G.H., Karlén, W., 1973. Holocene climatic variations—their pattern and possible cause. Quaternary Research 3, 155–205.

Enting, I.G., 1987. On the use of smoothing splines to filter CO_2 data. Journal of Geophysical Research—Atmospheres 92, 10977–10984.

Etheridge, D.M., Steele, L.P., Langenfelds, R.L., Francey, R.J., Barnola, J.-M., Morgan, V.I., 1996. Natural and anthropogenic changes in atmospheric CO_2 over the last 1000 years from air in Antarctic ice and firn. Journal of Geophysical Research 101, 4115–4128.

Field C.V., Schmidt, G.A., Koch, D., Salyk, C., 2006. Modeling production and climate-related impacts on ^{10}Be concentration in ice cores. Journal of Geophysical Research 111.

Gleeson, L.J., Axford, W.I., 1968. Solar modulation of galactic cosmic rays. Astrophysical Journal 154, 1011–1018.

Hoyt, D.V., Schatten, K.H., 1998. Group sunspot numbers: a new solar activity reconstruction. Solar Physics 179, 189–219.

Joos, F., 1994. Imbalance in the budget. Nature 370, 181–182.

Joos, F., Bruno, M., 1998. Long-term variability of the terrestrial and ocean carbon sinks and the budgets of the carbon isotopes ^{13}C and ^{14}C. Global Biochemical Cycles 12, 277–295.

Joos, F., Bruno, M., Fink, R., Stocker, T.F., Siegenthaler, U., Le Quéré, C., Sarmiento, J.L., 1996. An efficient and accurate representation of complex oceanic and biospheric models of anthropogenic carbon uptake. Tellus 48B, 397–417.

Korte, M., Constable, C.G., 2005. Continuous geomagnetic field models for the past 7 millennia: 2. CALS7K. Geochemistry, Geophysics, Geosystems 6.

Lal, D., Peters, B., 1967. Cosmic ray produced radioactivity on the Earth. In: Flügge, S. (Ed.), Handbuck der physik, vol. 46/2. Springer, Berlin, pp. 551–612.

Lean, J., Beer, J., Bradley, R., 1995. Reconstruction of solar irradiance since 1610: implications for climate change. Geophysical Research Letters 22, 3195–3198.

Marchal, O., Stocker, T.F., Joos, F., 1998. A latitude-depth, circulation-biogeochemical ocean model for paleoclimate studies. Development and sensitivities. Tellus 50B, 290–316.

Marland, G., Boden, T.A., Andres, R.J., 2003. Global, regional, and national CO_2 emissions. In: Global, Regional, and National CO_2 Emissions. US Department of Energy, Oak Ridge, Oak Ridge, TN, USA.

Masarik, J., Beer, J., 1999. Simulation of particle fluxes and cosmogenic nuclide production in the Earth's atmosphere. Journal of Geophysical Research 104, 12099–12111.

McCormac, F.G., Hoog, A.G., Blackwell, P.G., Buck, C.E., Higham, T.F.G., Reimer, P.J., 2004. SHCAL04 Southern Hemisphere Calibration, 0–11.0 CAL KYR BP. Radiocarbon 46 (3), 1087–1092.

McCracken, K.G., 2004. Geomagnetic and atmospheric effects upon the cosmogenic ^{10}Be observed in polar ice. Journal of Geophysical Research 109, A04101.

McCracken, K.G., Heikkila, B., 2003. The cosmic ray intensity between 1933 and 1965. In: Kajita, T., Asaoka, Y., Kawachi, A., Matsubara, Y., Sasaki, M. (Eds.), The Cosmic Ray Intensity Between 1933 and 1965. Universal Academy Press, Inc., pp. 4117–4120.

McCracken, K.G., McDonald, F.B., Beer, J., Raisbeck, G.M., Yiou, F., 2004. A phenomenological study of the long-term cosmic ray modulation, 850–1958 AD. Journal of Geophysical Research 109, A12103.

McHargue, L.R., Damon, P.E., 1991. The global beryllium 10 cycle. Reviews of Geophysics 29 (2), 141–158.

Müller, S.A., Joos, F., Edwards, N.R., Stocker, T.F., in press. Water mass distribution and ventilation time scales in a cost-efficient, 3-dimensional ocean model. Journal of Climate.

Muscheler, R., 2000. Nachweis von Änderungen im Kohlenstoffkreislauf durch Vergleich der Radionuklide ^{10}Be, ^{36}Cl und ^{14}C, Ph.D. Thesis, ETH Zurich, No. 13941.

Muscheler, R., Beer, J., Vonmoos, M., 2004a. Causes and timing of the 8200 yr BP event inferred from the comparison of the GRIP ^{10}Be and the tree ring Δ^{14}C record. Quaternary Science Reviews. Special issue Holocene climate variability—a marine perspective edited by E. Jansen, P. deMenocal and F. Grousset 23/20–22, pp. 2105–2115.

Muscheler, R., Beer, J., Wagner, G., Laj, C., Kissel, C., Raisbeck, G.M., Yiou, F., Kubik, P.W., 2004b. Changes in the carbon cycle during the last deglaciation as indicated by the comparison of ^{10}Be and ^{14}C records. Earth and Planetary Science Letters 219, 325–340.

Muscheler, R., Beer, J., Kubik, P.W., Synal, H.-A., 2005a. Geomagnetic field intensity during the last 60,000 years based on ^{10}Be & ^{36}Cl from the Summit ice cores and ^{14}C. Quaternary Science Reviews 23, 2101–2111.

Muscheler, R., Joos, F., Müller, S.A., Snowball, I., 2005b. How unusual is today's solar activity? Nature 436, E3–E4.

Orr, J.C., 1999. On ocean carbon-cycle model comparison. Tellus 51B, 509–510.

Raisbeck, G.M., Yiou, F., 2004. Comment on millennium scale sunspot number reconstruction: evidence for an unusually active sun since the 1940s. Physical Review Letters 92.

Raisbeck, G.M., Yiou, F., Fruneau, M., Loiseaux, J.M., Lieuvin, M., Ravel, J.C., 1981. Cosmogenic $^{10}Be/^{7}Be$ as a probe of atmospheric transport processes. Geophysical Research Letters 8, 1015–1018.

Raisbeck, G.M., Yiou, F., Jouzel, J., Petit, J.R., 1990. ^{10}Be and $\delta^{2}H$ in polar ice cores as a probe of the solar variability's influence on climate. Philosophical Transactions of the Royal Society of London Series A 330, 65–72.

Reimer, P.J., Baillie, M.G.L., Bard, E., Bayliss, A., Beck, J.W., Bertrand, C.J.H., Blackwell, P.G., Buck, C.E., Burr, G.S., Cutler, K.B., Damon, P.E., Edwards, R.L., Fairbanks, R.G., Friedrich, M., Guilderson, T., Hogg, A.G., Hughen, K.A., Kromer, B., McCormac, G., Manning, S., Bronk Ramsey, C., Reimer, R.W., Remmele, S., Southon, J., Stuiver, M., Talamo, S., Taylor, F.W., van der Pflicht, J., Weyhenmeyer, C.E., 2004. INTCAL04 terrestrial radiocarbon age calibration, 0–26 CAL KYR BP. Radiocarbon 46 (3), 1029–1058.

Siegenthaler, U., 1983. Uptake of excess CO_2 by an outcrop-diffusion model ocean. Journal of Geophysical Research 88, 3599–3608.

Siegenthaler, U., Oeschger, H., 1987. Biospheric CO_2 emissions during the past 200 years reconstructed by deconvolution of ice core data. Tellus 39B, 140–154.

Siegenthaler, U., Joos, F., 1992. Use of a simple model for studying oceanic tracer distributions and the global carbon cycle. Tellus 44B, 186–207.

Siegenthaler, U., Heimann, M., Oeschger, H., 1980. ^{14}C variations caused by changes in the global carbon cycle. Radiocarbon 22, 177–191.

Siegenthaler, U., Monnin, E., Kawamura, K., Spahni, R., Schwander, J., Stauffer, B., Stocker, T.F., Barnola, J.-M., Fischer, H., 2005. High resolution CO_2 records over the last 1000 years from the EPICA Dronning Maud Land ice core. Tellus 57B, 51–57.

Snowball, I., Sandgren, P., 2002. Geomagnetic field variations in northern Sweden during the Holocene quantified from varved lake sediments and their implications for cosmogenic nuclide production rates. The Holocene 12 (5), 517–530.

Solanki, S.K., Schüssler, M., Fligge, M., 2000. Evolution of the Sun's large-scale magnetic field since the Maunder minimum. Nature 408, 445–447.

Solanki, S.K., Usoskin, I.G., Kromer, B., Schüssler, M., Beer, J., 2004. Unusual activity of the Sun during recent decades compared to the previous 11,000 years. Nature 431, 1084–1087.

St-Onge, G., Stoner, J.S., Hillaire-Marcel, C., 2003. Holocene paleomagnetic records from the St. Lawrence Estuary, eastern Canada: centennial-to millennial-scale geomagnetic modulation of cosmogenic isotopes. Earth and Planetary Science Letters 209, 113–130.

Stuiver, M., Polach, H.A., 1977. Discussion: reporting of ^{14}C data. Radiocarbon 19, 355–363.

Stuiver, M., Quay, P.D., 1980. Changes in atmospheric Carbon-14 attributed to a variable sun. Science 207, 11–19.

Stuiver, M., Braziunas, T.F., 1993. Sun, ocean, climate and atmospheric $^{14}CO_2$, an evaluation of causal and spectral relationships. The Holocene 3, 289–305.

Stuiver, M., Reimer, P.J., Braziunas, T.F., 1998. High-precision radiocarbon age calibration for terrestrial and marine samples. Radiocarbon 40, 1127–1151.

Suess, H.E., 1953. Natural Radiocarbon and the Rate of exchange of carbon dioxide between the atmosphere and the Sea. In: Nuclear Processes in Geologic Settings (Ed.), National Research Council Committee on Nuclear Science (Washington, DC: National Academy of Sciences), University of Chicago Press, Chicago, pp. 52–56.

Usoskin, I.G., Mursula, K., Solanki, S.K., Schüssler, M., Kovaltsov, G.A., 2002. A physical reconstruction of cosmic ray intensity since 1610. Journal of Geophysical Research 107.

Usoskin, I.G., Solanki, S.K., Schüssler, M., Mursula, K., Alanko, K., 2003. A millennium scale sunspot number reconstruction: evidence for an unusually active sun since the 1940s. Physical Review Letters 91, 211101-1-4.

Valet, J.-P., 2003. Time variations in geomagnetic intensity. Reviews of Geophysics 41, 4/1–4/44.

Wagner, G., Beer, J., Laj, C., Kissel, C., Masarik, J., Muscheler, R., Synal, H.-A., 2000. Chlorine-36 evidence for the Mono Lake event in the Summit GRIP ice core. Earth and Planetary Science Letters 181, 1–6.

Wagner, G., Laj, C., Beer, J., Kissel, C., Muscheler, R., Masarik, J., Synal, H.-A., 2001. Reconstruction of the paleoaccumulation rate of central Greenland during the last 75 kyr using the cosmogenic radionuclides ^{36}Cl and ^{10}Be and geomagnetic field intensity data. Earth and Planetary Science Letters 193, 515–521.

Webber, W.R., Higbie, P.R., 2003. Production of cosmogenic Be nuclei in the Earth's atmosphere by cosmic rays: Its dependence on solar modulation and the interstellar cosmic ray spectrum. Journal of Geophysical Research 108 (A9), 1355.

Yang, S., Odah, H., Shaw, J., 2000. Variations in the geomagnetic dipole moment over the last 12,000 years. Geophysical Journal International 140, 158–162.

Yiou, F., Raisbeck, G.M., Baumgartner, S., Beer, J., Hammer, C., Johnsen, S., Jouzel, J., Kubik, P.W., Lestringuez, J., Stiévenard, M., Suter, M., Yiou, P., 1997. Beryllium 10 in the Greenland Ice Core Project ice core at Summit, Greenland. Journal of Geophysical Research 102, 26783–26794.